S3.4 MESOSCALE CONVECTIVE SYSTEMS ASSOCIATED WITH AFRICAN EASTERLY WAVES

Matthew A. Janiga* and Chris D. Thorncroft
University at Albany, SUNY, Albany, NY

1. INTRODUCTION

African easterly waves (AEWs) are synoptic-scale disturbances, which modulate convection during the West African monsoon. The dominant form of convection associated with AEWs is organized mesoscale convective systems (MCSs). This is due to the presence of high CAPE and shear along the baroclinic zone separating the Sahara from the cool Gulf of Guinea.

Over the continent, moist convection is located ahead of the AEW trough (e.g., Fink and Reiner 2003; Kiladis et al. 2006). This has been associated with adiabatic forcing for ascent (Kiladis et al. 2006) and increased lower-tropospheric equivalent potential temperature (θ_e) (Berry and Thorncroft 2005). However, many previous studies of the relationship between AEWs and convection are based on simple measurers of convection such as OLR (e.g., Kiladis et al. 2006).

We examine how the characteristics of convection depicted by the Tropical Rainfall Measuring Mission (TRMM) Precipitation Radar (PR) vary as a function of AEW phase. AEW phase is determined using a wavenumber-frequency filtering technique similar to Riley et al. (2011). To interpret these results, reanalysis grids were are also composited by AEW phase.

2. DATA

The TRMM 3B42 product (Huffman et al. 2007) provides precipitation estimates on a fixed 0.25° grid at regular 3 h intervals. The TRMM PR (products 2A23 and 2A25 version 7) measures vertical profiles of reflectivity; this data is used to estimate the surface rain rate and convective/stratiform designations (TSDIS 2011). The TRMM PR has a horizontal resolution of approximately 5 km and a vertical resolution of 250 m (the boosting of the satellite in August of 2001 slightly reduced the horizontal resolution).

The variation of thermodynamic and kinematic properties as a function of wave phase were determined using the NCEP Climate Forecast System Reanalysis (CFSR, Saha et al. 2010). These reanalyses are available every 6 h on a fixed 0.5° grid.

* *Corresponding author address:* Matthew A. Janiga, Univ. at Albany, Dept. of Atmospheric and Environmental Science, Albany, NY 12222; e-mail: janiga@atmos.albany.edu.

3. METHODOLOGY

The TRMM 3B42 precipitation associated with AEWs was determined using a wavenumber-frequency filter. Periods of 2.5-10 days and wavenumbers between -20 to -7 (wavelengths of 2000-5600 km) were retained. This is comparable to what has been used in previous studies of AEWs (e.g., Kiladis et al. 2006) and is sometimes referred to as the tropical-depression (TD) band.

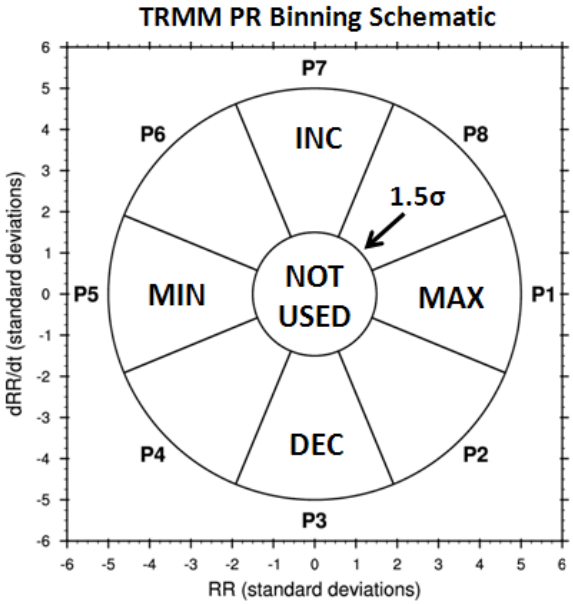

Figure. 1 The TRMM PR binning procedure.

AEW phase and amplitude were determined using the standardized AEW filtered TRMM 3B42 (RR) and its standardized time derivative (dRR/dt). Standardized anomalies were calculated over JAS 1998-2010. AEW amplitude is the distance from the origin of Fig. 1; only amplitudes greater than 1.5 σ are utilized. 8 AEW phases were determined by both RR and dRR/dt. Phase 1 (5) represents the center of the convective envelope (suppressed region); phase 7 (3) represents increases (decreases) in AEW filtered TRMM 3B42.

To produce composites of the PR rain rate (shown in Fig. 2) the total, convective, and stratiform rain rate were first binned to a 1.0° grid matching the filtered TRMM 3B42 grid. Then those binned orbital data grids meeting the amplitude and phase constraints in Fig. 1 for each phase sector were binned together.

AEW phase composites were also produced using precipitation features (PFs). We define PFs as contiguous regions of non-zero PR rain rate. Similar to the procedure above, the rain rate from PFs at several size intervals were binned to a 1.0° grid matching the filtered TRMM 3B42 grid and then averaged over each phase sector.

Contoured frequency altitude diagram (CFAD) composites were produced for each AEW phase for reflectivity profiles with non-zero convective and stratiform PR rain rates (shown in Fig. 3). Again, data was binned to 1.0° grid to determine wave phase and amplitude. At each vertical level and for each AEW phase, we determine the percent frequency of occurrence for each reflectivity value. The CFAD composites for each AEW phase were normalized so that the sum of all the values is the same. For each of the phases, the difference in reflectivity occurrence between that phase and the composite is plotted.

For the reanalysis composites, the CFSR analyses were first interpolated to a grid matching the filtered TRMM 3B42. Then phase and amplitude were determined and the CFSR data was binned and averaged for each phase sector. All of the calculations in Fig. 2-4 were performed over the domain 5-15°N, 10°W-10°E and the period JAS 1998-2010.

4. RESULTS

Figure 2a shows the dependence of rain rate—determined by the PR—on AEW phase. By design, high rain rates are found in phase 1 and low rain rates are found in phase 5. Figure 2a also shows an increase in stratiform fraction between the leading edge (phase 7) and the trailing edge (phase 3) of the AEW convective envelope. The conditional convective rain rate is an average which excludes zeros and it is slightly higher in phase 1 than the other phases (Fig. 2b). The conditional rain rate is indicative of the intensity of convection. Figure 2c shows that increases in rain coverage play a more important role than rain intensity in determining the variation of rain rate with phase.

Figure 2d is a 2D histogram which shows the contribution of various PF sizes in each AEW phase to the total volumetric rainfall in all phases. A PF area of 10,000 km^2 can generally be associated with MCSs which are often defined as precipitation systems with a length greater than 100 km in one dimension. Therefore, Fig. 2d shows that MCSs account for the majority of rainfall in the domain. It also shows that rainfall contributions from very large systems (area > 100,000 km^2) preferentially occur in phase 1.

Figure 3 shows CFAD diagrams for convective and stratiform rain for each of the AEW phases. The upper left panel of Fig. 3a and 3b show a CFAD composite constructed from all of the phases. In the convective CFAD composite, two frequency maxima are present below 4 km. The one between 20-25 dBZ is associated with shallow warm rain and the one between 35-40 dBZ is associated with deep convection. In the stratiform CFAD composite, there is a kink between 4-5 km associated with a bright band. In the rest of the panels, deviations from the composite are shaded and the composite is outlined in a thin black contour.

For convective precipitation, the main difference between phases is the relative frequency of the deep and shallow convective modes (Fig. 3a). The shallow mode is relatively more frequent in the suppressed phases (3 to 7) and the deep mode is more frequent in the enhanced phases (8, 1, and 2). For stratiform precipitation, higher reflectivity values are more common in the enhanced phases (Fig. 3b). In addition, the enhanced phases show more vertical development above the melting layer (above 4.5 km).

Figure 4 shows AEW phase-altitude composites of vorticity, zonal wind, specific humidity, and θ_e. Anomalies are defined as the deviation from the average across all phases.

There are cyclonic vorticity anomalies in phases 2 and 3 indicating the position of the trough; anticyclonic vorticity anomalies in phases 6 and 7 indicate the position of the ridge. The amplitude of the trough peaks at 700-600 hPa consistent with previous studies and a cold-core structure. Temperature anomalies also confirm the cold-core structure (not shown). Phase 1 is located ahead or west of the trough confirming previous studies which found convection ahead of the trough.

The climatological wind at 700-600 hPa (below 850 hPa) is easterly (westerly). Therefore, the zonal wind anomalies indicate increased zonal shear in phases 1 and 8 and reduced shear in phases 4 and 5 (Fig. 4b). Positive anomalies of specific humidity and θ_e are also observed ahead of the trough where convection is enhanced; unfavorable thermodynamic conditions are found in the suppressed phases (Fig. 4c, d).

5. DISCUSSION AND CONCLUSIONS

A tendency for more intense rainfall, larger PFs, and deeper moist convection was found in the enhanced phases of AEWs relative to the suppressed phases. The convective envelope was located ahead of the AEW trough consistent with previous studies. Ahead of the AEW trough, there were increases in zonal shear, middle-tropospheric moisture, and lower-tropospheric θ_e. These factors are consistent with the overall increase in convective intensity ahead of the trough.

There was also a transition from shallow convective to deep convective to stratiform precipitation from phase 7 to phase 3. The transition from shallow convective to deep convective precipitation appears to coincide with a moistening of the middle-troposphere. The reduced intensity of convection in phases 4-6 can be attributed to several

factors. There is adiabatic forcing for descent below the AEJ behind the trough (e.g., Kiladis et al. 2006). In addition, there is drying in the middle-troposphere, which may be associated with subsidence. Furthermore, there is reduced zonal shear east of the AEW trough and lower-tropospheric cooling.

ACKNOWLEDGMENTS

This work was supported by NSF grant ATM0732255.

REFERENCES

Berry, G. J., and C. Thorncroft. 2005. Case study of an intense African easterly wave. *Mon. Wea. Rev.* **133**, 752–766.

Fink, A. H., and A. Reiner, 2003: Spatiotemporal variability of the relation between African Easterly Jets and and West African squall lines in 1998 and 1999. *J. Geophys. Res.*, **108**, 4332, doi:10.1029/2002JD002816.

Huffman, G. J., and Coauthors, 2007: The TRMM Multisatellite Precipitation Analysis (TMPA): Quasi-global, multiyear, combined-sensor precipitation estimates at fine scales. *J. Hydrometeor.*, **8**, 38–55.

Kiladis, G. N., C. D. Thorncroft, and N. G. Hall, 2006: Three-dimensional structure and dynamics of African easterly waves. Part I: Observations. *J. Atmos. Sci.*, **63**, 2212–223

Riley, E. M., B. Mapes, and S. N. Tulich, 2011: Clouds associated with the Madden–Julian oscillation: A new perspective from CloudSat. *J. Atmos. Sci.*, **68**, 3032–3051.

Saha, S., and Coauthors, 2010: The NCEP Climate Forecast System Reanalysis. *Bull. Amer. Meteor. Soc.*, **91**, 1015–1057.

TSDIS, 2011: *File Specifications for TRMM Products—Version 7*. [Available online at ftp://pps.gsfc.nasa.gov/pub/v7filespec/filespec.TRMM.V7.pdf]

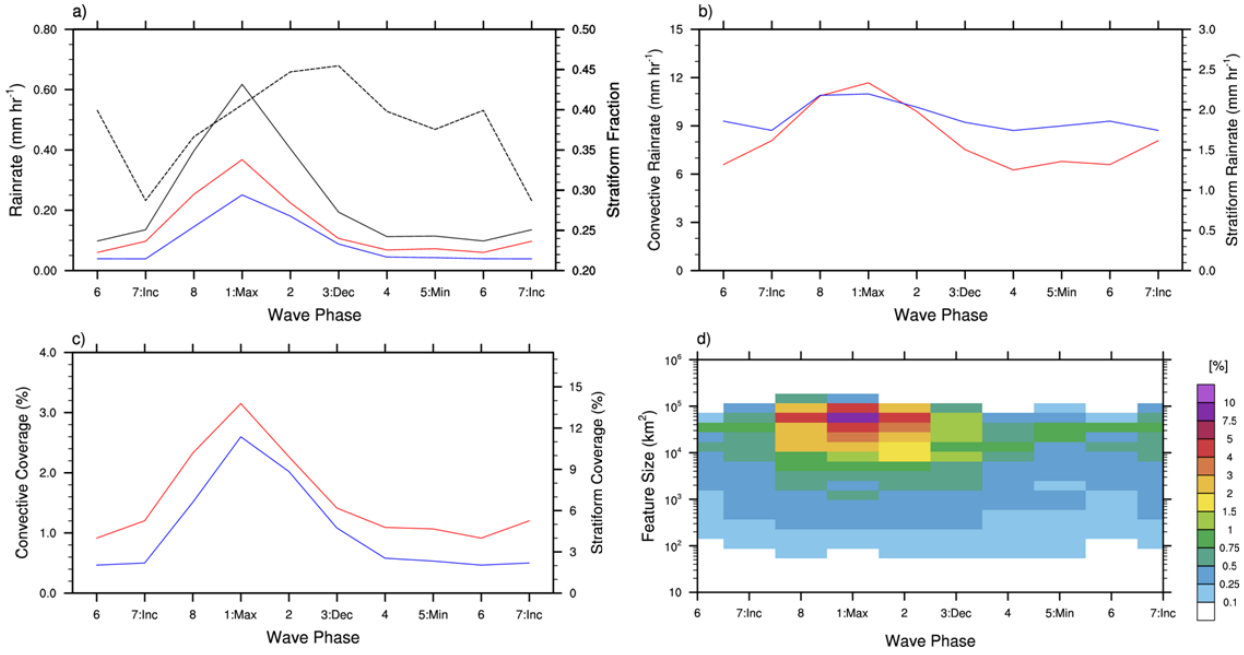

Figure 2. (a) Unconditional total (black), convective (red), stratiform (blue) rain rate (mm hr^{-1}) and stratiform fraction (dashed) (b) conditional convective (red) and stratiform (blue) rain rate (mm hr^{-1}) (c) convective (red) and stratiform (blue) fractional area coverage (%) (d) 2D histogram of contributions (%) to the total rainfall from different PF size and wave phase bins.

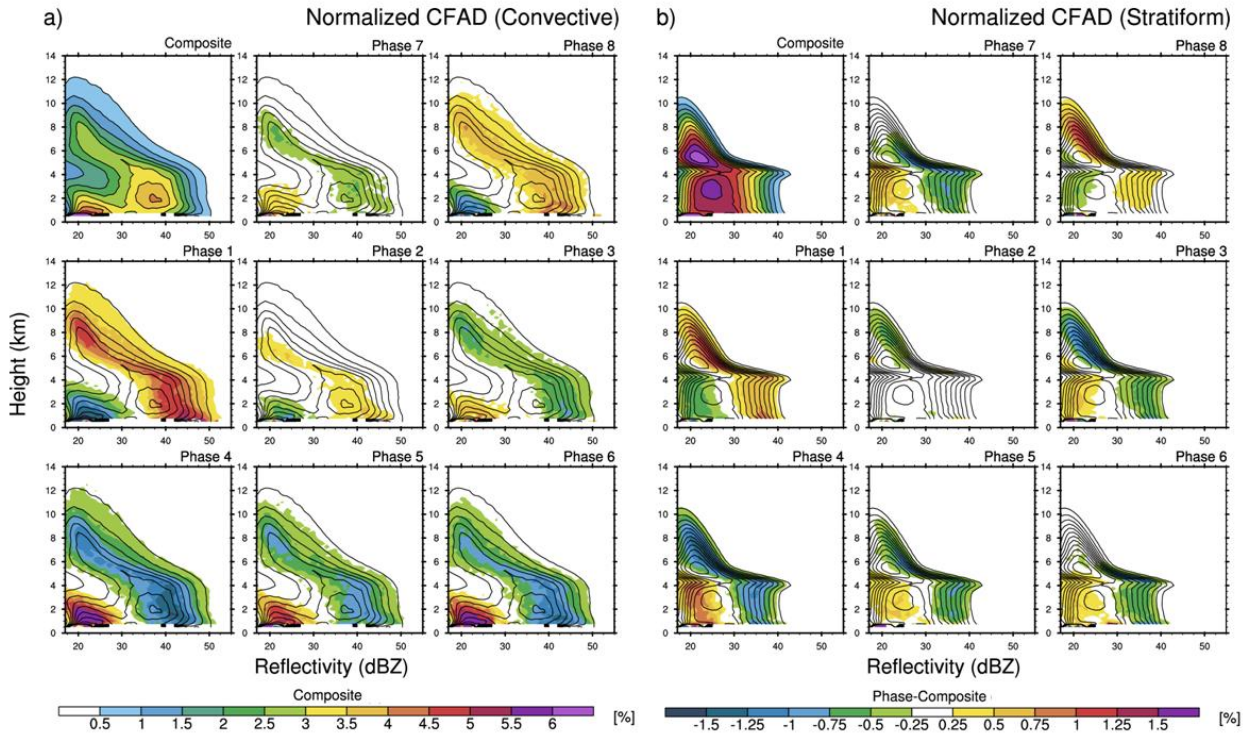

Figure 3. Normalized CFAD diagrams for the all-phase composites (upper-left) and differences between the composite and each phase (other panels) for (a) convective (b) stratiform precipitation. The units are frequency of occurrence (%) which is defined at each level.

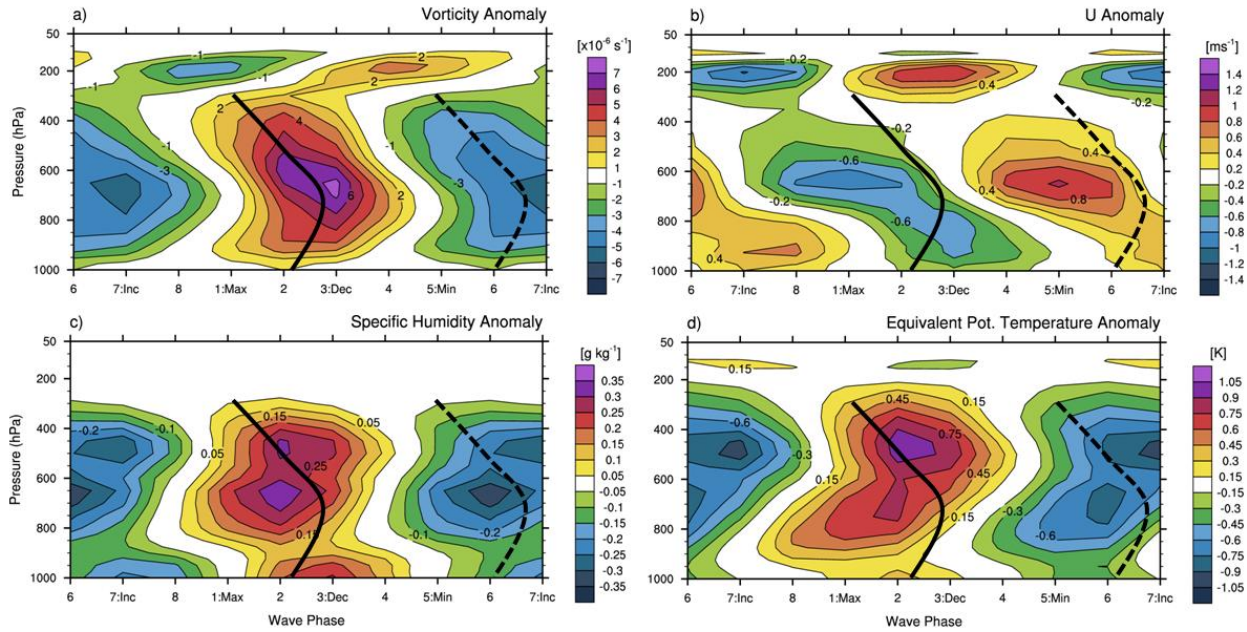

Figure 4. AEW phase-altitude plots of anomalies of (a) vorticity ($x10^{-6}$ s^{-1}) (b) zonal wind (m s^{-1}) (c) specific humidity (g kg^{-1}) (d) equivalent potential temperature (K) from the CFSR. The trough (ridge) axis is shown by the solid (dashed) line.